# Indenter-Foam Dampers Inspired by Cartilage: Dynamic Mechanical Analyses and Design

Guebum Han

Postdoctoral Researcher

Mechanical Engineering, University of Minnesota

111 Church St SE, Minneapolis, MN 55455

Email: ghan@umn.edu

Utku Boza

Mechatronics Engineer

ASML Research and Development

De Run 6501, 5504 DR Veldhoven, Netherlands

Email: <u>utkuboz87@gmail.com</u>

Lejie Liu

Graduate Student

Mechanical Engineering, University of Wisconsin-Madison

1513 University Ave, Madison, Wisconsin 53706, USA

Email: <u>lliu265@wisc.edu</u>

Corinne R. Henak

Assistant Professor

Mechanical Engineering, University of Wisconsin-Madison

1513 University Ave, Madison, Wisconsin 53706, USA

Biomedical Engineering, University of Wisconsin-Madison

1550 University Ave, Madison, WI 53706, USA

Email: <a href="mailto:chenak@wisc.edu">chenak@wisc.edu</a>

Melih Eriten

Associate Professor

Mechanical Engineering, University of Wisconsin-Madison

1513 University Ave, Madison, Wisconsin 53706, USA

Email: eriten@wisc.edu

Abstract

Articular cartilage is a thin layer of a solid matrix swollen by fluid, and it protects joints from

damage via poroviscoelastic damping. Our previous experimental and simulation studies showed

that cartilage-like poroviscoelastic damping could widen the range of damping methods in a low-

frequency range (< 100 Hz). Thus, the current study aimed to realize cartilage-like damping

capacity by single- and two-indenter-foam poroviscoelastic dampers in a low-frequency range.

Multiple single-indenter-foam dampers were designed by combining foam sheets with different

pore diameters and indenters with different radii. Their damping capacity was investigated by

dynamic mechanical analysis in a frequency range of 0.5 - 100 Hz. Single-indenter-foam dampers

delivered peak damping frequencies that depended on the foam's pore diameter and characteristic

diffusion length (contact radii). Those dampers maximize the damping capacity at the desired

frequency (narrowband performance). A mechanical model combined with simple scaling laws

was shown to relate poroelasticity to the peak damping frequencies reasonably well. Finally,

combinations of single-indenter-foam dampers were optimized to obtain a two-indenter-foam

damper that delivered nearly rate-independent damping capacity within 0.5 – 100 Hz (broadband

performance). These findings suggested that cartilage-like poroviscoelastic dampers can be an

effective mean of passive damping for narrowband and broadband applications.

**Keywords:** Poroviscoelasticity, cartilage dissipation, tunable peak damping frequency, broadband

damping

2 Eriten VIB-20-1073

## 1. INTRODUCTION

Structures in aerospace, marine, automotive, and manufacturing industries undergo broadband vibrations and noise, which can cause material and component failure and occupational health hazards. Various techniques are available in the literature to suppress undesired vibrations and noise [1–4]. Passive methods offer robust, effective, and stable performance at relatively high frequencies, but their suppression capacity generally drops at relatively low frequencies (< 100 Hz) [5,6]. Several remedies to this reduction were proposed in the literature. For instance, Xue et al. simulated a thick layer of poroelastic materials on thin aluminum plates and demonstrated uncompromised damping capacity for low-frequencies (<100 Hz) [7]. However, this treatment utilized a passive layer with thickness 30 times that of the plate. Noting the practical challenges of such treatments, previous works had proposed adding auxiliary passive absorbers to poroelastic layers [6,8]. In general, embedding such auxiliary energy storing and dissipating systems to a host structure enhances low-frequency performance (e.g., distributed vibration absorbers). Novel materials and optimization techniques are currently available for the optimal design of these absorbers. For instance, Zuo and Nayfeh proposed a robust single degree-of-freedom (DOF) absorber by treating stiffness and damping values as control variables [9]. They also showed that a 2-DOF tuned mass-spring-damper system performed better than the single DOF system in vibration suppression [10]. In addition, previous studies showed that optimizing the frequency distribution of oscillators provided satisfactory vibration suppression [11] and nearly irreversible energy transfer [12]. Carcaterra et al. [13] demonstrated the efficacy of oscillators on a satellite (UNISAT). However, typical limitations of undamped oscillators are a possible reversal of vibration energy to the host, leading to their early failure [14].

Interfacial and material damping mechanisms can overcome the limitations of undamped oscillators [15]. Interfacial damping involves mechanical losses due to frictional slip, microscale impacts, and relaxations localized to contact interfaces [16]. A typical example of interfacial damping is the underplatform dampers used to reduce resonances in blades of a gas turbine [17]. Rate-independent frictional interactions constitute the major mechanism of energy losses in these dampers. Material damping is dominantly observed in viscoelastic materials [18]. In particular, viscoelastic materials have been employed in sandwiched [19] and composite structures [20] to enhance damping. Bitumen-based viscoelastic damping is heavily used in automotive frames, aircraft fuselages [21], and ship decks [22]. Granular viscoelastic materials can provide the maximum damping at a targeted frequency range by using different properties of particles [23]. Although viscoelastic materials help overcome the challenges of undamped oscillators, they exhibit narrow bandwidth [18] and place maximum damping at relatively high frequencies. Therefore, they might not be useful for low structural modes (< 100 Hz) [24].

Effective damping efficacy of synthetic noise-absorbing materials is primarily limited to relatively high frequencies (> 100 Hz), and therefore recent efforts to expand the bandwidth in low frequencies were made by adding active and passive systems [5]. For example, Harne et al. attached a thin plate to a poroelastic foam layer to attenuate low-frequency vibrations [25]. Embedding mass inclusions with low resonance frequencies into a poroelastic matrix was another solution to the bandwidth problem [8]. These inclusions were designed to move significantly and thus increased damping due to inclusion-matrix interactions at low-frequency resonances. Composite dampers combined with poroelastic damping could achieve effective damping at both ends of the frequency spectrum. Deshmukh and McKinley proposed poroviscoelastic (PVE)

Eriten 4 VIB-20-1073

composites (open-cell polyurethane foam with magnetorheological fluid) as an adaptive energy-absorbing material [26].

Articular cartilage, composed of a dense solid matrix swollen by fluid, exhibits effective damping in a low-frequency range of less than 100 Hz. Effective cartilage damping in the lowfrequency range stems from the combination of poroelastic and viscoelastic damping mechanisms [27]. Poroelastic damping stems from solid-fluid friction interactions in cartilage, and viscoelastic damping originates from the rearrangements of the solid fibrillary [28–30]. Therefore, poroelastic damping is dependent on the diffusivity and characteristic diffusion length in loading [27,31,32], but viscoelastic damping is length-independent. Our previous study about cartilage damping mechanisms (5 - 100 Hz) [27] showed that viscoelastic damping in cartilage provided base damping independent of characteristic diffusion lengths in loading, and poroelastic damping provided additional damping at a relatively small characteristic diffusion length in loading. Besides, our other past studies about cartilage-like dampers numerically showed that characteristic diffusion lengths in loading could be optimized to achieve rate-independent damping and maximum damping at desired frequencies (3-3000 Hz) [33,34]. These experimental [27,32,35] and simulation studies [33,34] inspired the development of cartilage-like dampers combined with multiple diffusion lengths in loading to provide effective and sustained damping in a lowfrequency range (< 100 Hz). These potential benefits are a driving force behind this study. This damping method can be categorized as a hybrid of interfacial and material damping and fills in the deficiency of damping methods for a low-frequency range.

This study aims to demonstrate a practical realization of cartilage-inspired PVE dampers that provide maximum damping at desired frequencies and rate-independent broadband damping in a relatively low-frequency range (< 100 Hz). Cartilage-inspired PVE dampers are designed with

Eriten 5 VIB-20-1073

indenter-foam configurations for a low-frequency range of 0.5 - 100 Hz. The PVE dampers in a single-indenter-foam configuration (singe diffusion length in loading) are investigated through dynamic mechanical analysis (DMA) to quantify the effects of indenter radii and mean pore sizes on their damping capacity and show the ability to place maximum damping at desired frequencies (narrowband performance). Based on the results of single-indenter-foam dampers, we design and test the optimized PVE damper in a two-indenter-foam configuration (two diffusion lengths in loading) that provides nearly rate-independent damping capacity (broadband performance). Section 2 summarizes our recent findings on effective cartilage PVE dissipation in a low-frequency range, conducts a scaling analysis to be used in the designs and analyses of cartilage-inspired foam-indenter dampers, and presents the experimental details on the DMA of the dampers. Section 3 presents the damping performance of single- and two-indenter-foam dampers. Section 4 discusses the assumptions used in the scaling analysis and challenges before the actual implementation of cartilage-inspired PVE dampers on real structures. Section 5 concludes this study with a summary of the findings.

## 2. THEORY AND METHODS

## 2.1 PVE Damping of Cartilage

Our previous work uncoupled cartilage damping mechanisms by using the dependence of poroelastic damping on a characteristic diffusion length involved in the mechanical load on the tissue (Figure 1) [27]. The characteristic length was a contact radius between a rigid indenter and hydrated cartilage (Figure 1a). Phase lags  $\delta$  between applied strains and measured stresses were measured at different contact radii;  $\delta$  is a measure of damping and can be converted into the specific damping capacity  $\varphi = 2\pi \tan \delta$  [18]. The frequency  $f_{peak}$  at which the phase lag attains a maximum value due to the maximized poroelastic damping was governed by the combination of

the diffusivity of a material  $\beta$  and contact radius a ( $f_{peak} \sim \frac{\beta}{a^2}$ ) (Figure 1b) [27,32,35];  $f_{peak}$  is referred to as a poroelastic peak damping frequency in the next subsection, and  $\beta$  represents the diffusion rate of a solvent in a porous media. This result indicated that damping at a targeted frequency can be maximized by placing  $f_{peak}$  at the targeted frequency via the adjustment of  $\beta$  and  $\alpha$ . The previous study also showed that viscoelastic damping can provide base damping regardless of contact radii.

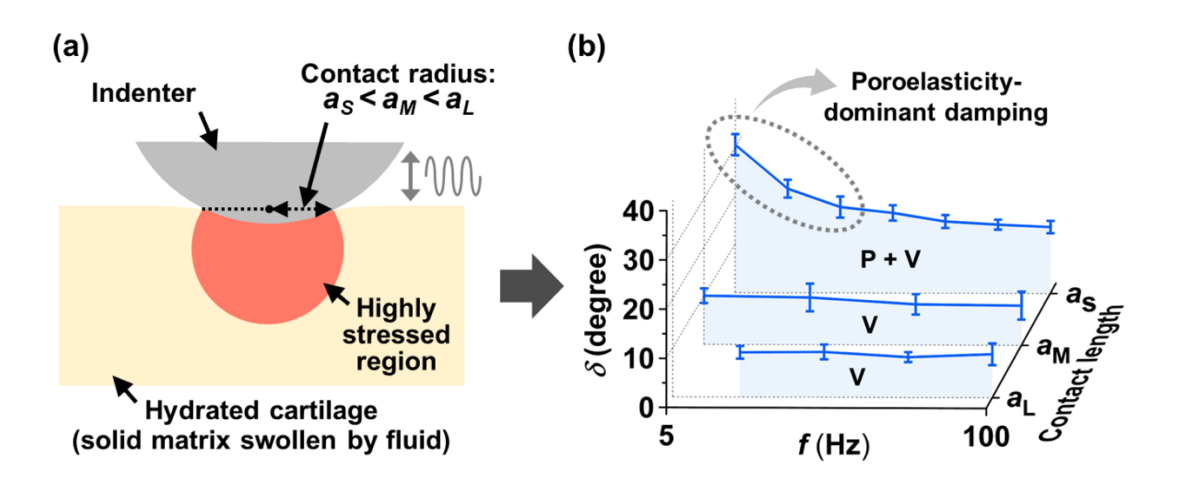


Figure 1 (a) Experimental setup for cartilage damping measurement and (b) results of cartilage damping (P: poroelastic damping and V: viscoelastic damping) at different characteristic lengths ( $a_S$ : ~13 µm,  $a_M$ : ~33 µm, and  $a_L$ : ~43 µm). Effective cartilage damping in a frequency range of 5 – 100 Hz originates from the combination of poroelastic and viscoelastic damping mechanisms. While viscoelastic damping provides sustained base damping regardless of contact radii ( $a_S$ ,  $a_M$ , and  $a_L$ ), poroelastic damping additionally increases damping at a relatively small contact radius ( $a_S$ ). The poroelastic peak damping frequency  $f_{peak}$  is governed by the diffusivity of a material  $\beta$  and contact radius a ( $f_{peak} \sim \frac{\beta}{a^2}$ ) [27,32,35]. This figure is not drawn to scale.

# 2.2 Analyses and Designs of Indenter-Foam Damper

We first design an indenter-foam damper that mimics cartilage-like PVE damping mechanisms.

The damper consists of a flat-ended cylindrical rigid indenter pressed on a viscoelastic foam sheet

swollen with a Newtonian liquid (Figure 2a). A characteristic diffusion length in an indenter-foam damper is controlled by changing a contact radius a between an indenter and a foam sheet, similar to our previous study about cartilage dissipation mechanisms (Section 2.1). Contact loading creates a gradient-stress profile that leads to large volumetric strains in the vicinity of the contact region and relatively low strains far from the contact region. These volumetric strains cause liquid diffusion and hence poroelastic losses (solid-fluid frictional interaction) close to the contact region. Viscoelastic damping of the foam is responsible for energy dissipation close to and far from the contact region. However, indentation-induced shear strains are generally significantly smaller than volumetric strains, and so are viscoelastic losses [40]. A simple mechanical model of this indenterfoam system neglecting viscoelastic losses is given in Figure 2b. In this model, the highly stressed region close to the contact region is modeled as a linear elastic zone with Young's modulus E combined with poroelastic damping  $\eta_l$ ; where  $\eta_l$  stems from the solid-liquid interaction (Kelvin-Voigt material). The region surrounding the highly stressed zone is modeled as linear elastic with the same Young's modulus of solid foam E because poroelastic interactions away from the contact are negligible due to diffused stresses. Thus, a standard linear solid element could represent the total response of the indenter-foam system. Small vibration amplitudes are assumed in the mechanical model of the indenter-foam system. Imposing harmonic loading with single frequency  $\omega$  in the form of harmonic stress  $\sigma = \sigma_M e^{i\omega t}$  (or strains  $\varepsilon = \epsilon_M e^{i\omega t}$ ;  $\varepsilon_0 = \epsilon_0 e^{i\omega t}$ ) in the following constitutive relations:

$$\sigma = E(\varepsilon - \varepsilon_0) + \eta_l(\dot{\varepsilon} - \dot{\varepsilon}_0) = E\varepsilon_0. \tag{1}$$

This simple model yields two constitutive relations:

$$\sigma_{M} = (E + i\omega\eta_{I})(\epsilon_{M} - \epsilon_{0}) = E\epsilon_{0}, \tag{2}$$

where  $\sigma_M$  and  $\epsilon_M$  are the steady-state amplitudes of stress and strain at the foam-indenter contact, respectively, and  $\epsilon_0$  is the steady-state amplitude of strain at the end of the highly-stressed zone. Eliminating  $\epsilon_0$  using the equalities in Eq.(2) delivers

$$\sigma_{M} = \frac{E(E + i\omega\eta_{l})}{2E + i\omega\eta_{l}} \epsilon_{M},\tag{3}$$

which is the relation for total stress-strain response of the foam-indenter system. Since this relation is similar to a constitutive equation at the steady-state, the terms in front of  $\epsilon_M$  is referred to as dynamic modulus  $G(\omega) = \frac{\sigma_M}{\epsilon_M} = \frac{E(E+i\omega\eta_l)}{2E+i\omega\eta_l}$ . When normalized to the total foam modulus E/2, this modulus takes the following form:

$$G_N(\omega) = \frac{G(\omega)}{E/2} = \frac{1 + i\omega\tau_{PE}}{1 + i\omega\frac{\tau_{PE}}{2}}$$
(4)

where  $\tau_{PE} = \frac{\eta_l}{E}$  is the poroelastic relaxation time constants. The argument of the dynamic modulus yields the phase lag  $\delta$  between stress and strain as follows:

$$\delta(\omega) = \angle G_N(\omega) = \arctan \omega \tau_{PE} - \arctan \omega \frac{\tau_{PE}}{2}.$$
 (5)

The phase lag is a common measure of material damping [18] and is used to measure the damping capacity of the foam-indenter system; the specific damping capacity  $\varphi$  can be calculated from the phase lag ( $\varphi = 2\pi \tan \delta$ ) [18]. The phase lag given in Eq. (5) attains maximum at  $\omega_{peak} = 2\pi f_{peak} = \sqrt{2}/\tau_{PE}$ ; i.e., when loading period is around the poroelastic relaxation time constant.

Eriten 9 VIB-20-1073

In the remainder of this paper, we will refer to the loading frequency that yields the maximum phase lag and thus damping as a poroelastic peak damping frequency  $f_{peak}$ .

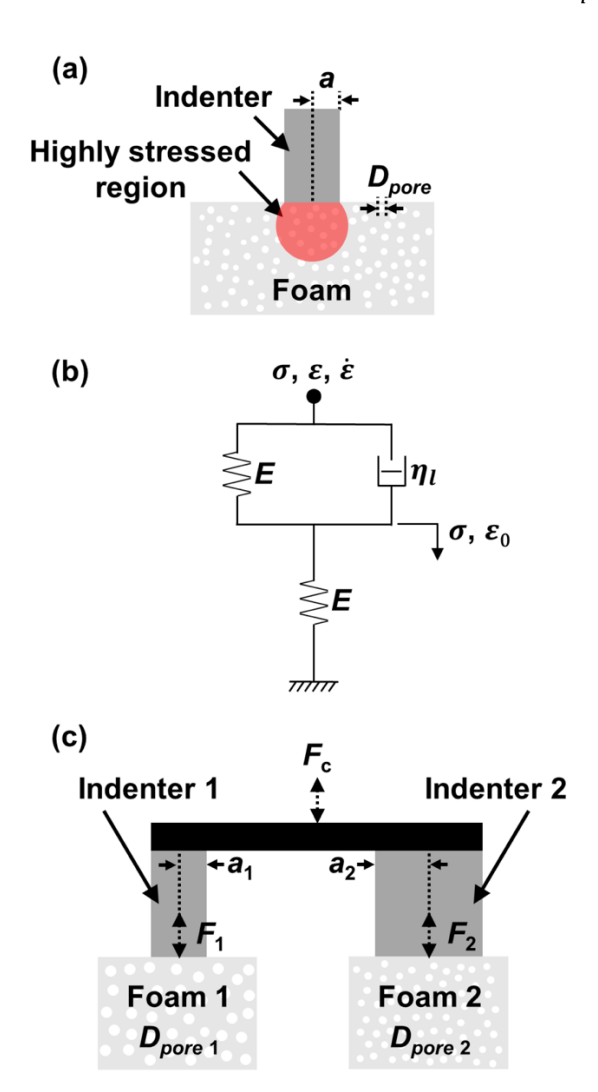


Figure 2 (a) Single-indenter-foam configuration, (b) its mechanical model, and (c) two-indenter-foam configuration. Foam sheets are swollen by fluid. The damping capacity of indenter-foam dampers, inspired by cartilage mechanisms, can be tuned by controlling the contact radius a, pore diameter  $D_{pore}$ , and the number of indenters. a is a characteristic diffusion length in an indenter-foam damper. This figure is not drawn to scale.

Next, we study the kinematics and swollen foam's response to the indenter oscillations in the vicinity of the contact region (i.e., highly stressed zone); obtain an expression for liquid damping coefficient  $\eta_l$  and thus relate the peak damping frequency to the physical properties of

the damper system (i.e.,  $f_{peak} \cong \frac{1}{\sqrt{2}\pi\tau_{PE}} = \frac{E}{\sqrt{2}\pi\eta_l}$ ). First, the highly stressed region in the vicinity of the rigid indenter is assumed to occupy a volume V that scales with the cube of indenter radius (i.e.,  $V \propto a^3$  as predicted by the linear elastic contact theories [36]). The rate of the volume change in that region due to the dynamic motion of the rigid indenter can be approximated as  $\frac{dV}{dt} \propto -\dot{\varepsilon}_{PE}a^3$ where compressive strain rates on the poroelastic dashpot  $\dot{\varepsilon}_{PE}$  are taken as positive. The average volumetric flux q and liquid velocity  $v_l$  out of that highly stressed zone scales with  $q \approx v_l \propto$  $\frac{1}{a^2} \frac{dV}{dt} \propto -\dot{\varepsilon}_{PE} a$ . Note that the high porosity in the foam and the incompressibility of the swelling liquid are inherently assumed in equating the flux to the liquid velocity. Assuming the diffusion of the liquid obeys Stokes' flow, Darcy's law relates stress-gradients to liquid velocity (i.e.,  $v_l \propto$  $-\frac{k}{\mu}\frac{\sigma_{PE}}{a}$ ). In this expression, k is the permeability of the foam (known to scale quadratically with the mean pore diameter  $D_{pore}$  in various foam sheets (i.e.,  $k \propto D_{pore}^2$  [37]),  $\mu$  is the dynamic viscosity of the swelling liquid, and  $\frac{\sigma_{PE}}{a}$  gives an estimate of gradients of stress carried by the poroelastic dashpot element. Relating the liquid velocity scaling from kinematics and the liquid diffusion yields the relation between the stress and strain rates on the poroelastic dashpot:

$$\sigma_{PE} \propto \mu \left(\frac{a}{D_{pore}}\right)^2 \dot{\varepsilon}_{PE}.$$
 (6)

Therefore, the liquid damping coefficient  $\eta_l \propto \mu \left(\frac{a}{D_{pore}}\right)^2$ , and so the peak damping frequency is found to scale as:

$$f_{peak} \cong \frac{E}{\sqrt{2}\pi\eta_I} \propto \frac{E}{\sqrt{2}\pi\mu} \left(\frac{D_{pore}}{a}\right)^2.$$
 (7)

Eriten 11 VIB-20-1073

Note that this scaling law can be rewritten as  $\frac{\beta}{a^2} = \frac{E}{\sqrt{2}\pi\mu} \left(\frac{D_{pore}}{a}\right)^2$  where  $\beta = \frac{ED_{pore}^2}{\sqrt{2}\pi\mu}$  is a measure of diffusivity in the foam. Therefore, the peak damping frequency obtained from the indenter-foam damper model obeys the same scaling with the peak damping frequency of cartilage. Beyond this highly stressed zone dominated by poroelastic losses, viscoelastic losses stemming from solid foam deformation provide baseline dissipation also observed in cartilage. Note that those losses are not accounted for in the simple mechanical model. Since viscoelastic losses do not exhibit length dependence, their contribution to peak-damping frequencies in the foam-indenter system is negligible. In conclusion, the indenter-foam system promises damping capacity similar to articular cartilage.

The scaling law obtained in Eq. (7) indicates that the peak damping frequency depends on material constants (the ratio of Young's modulus of the foam to the dynamic viscosity of the liquid) and geometric properties (the ratio of mean pore diameter to indenter radius). We choose to primarily vary the latter in the indenter-foam damper designs to confirm the tunability of the peak damping frequency in a range of 0.5 - 100 Hz, which results from the quadratic scaling with the geometric ratio  $\frac{D_{pore}}{a}$ .

Our recent numerical study showed that cartilage-like PVE dampers with multiple diffusion lengths in loading can offer rate-independent broadband damping [33]. Here, we experimentally validate this numerical study by designing a two-indenter-foam configuration (two diffusion lengths in loading) as shown in Figure 2c. Note that the panel connecting the two indenters is rigid, and the composite force  $F_c$  is treated as the vibration transmitted from a target structure to the two-indenter-foam damper. Consistent with our numerical work, we ensured that the indenters were sufficiently far from each other, the response of the foam was linear PVE so that it obeyed the same scaling law (Eq. (7)) as in the single-indenter case. Consequently, the

Eriten 12 VIB-20-1073

principle of superposition can be applied to the two-indenter-foam configuration. Therefore, the forces  $F_1$  and  $F_2$  carried by each indenter-foam configuration can be summed to obtain the composite force  $F_c$ . As the rigid indenters (Figure 2c) oscillate sinusoidally, the composite force can be represented as

$$F_c(\omega) = A_1(\omega)\sin(\omega t + \delta_1(\omega)) + A_2(\omega)\sin(\omega t + \delta_2(\omega)), \tag{8}$$

where  $A_1$  and  $A_2$  are the amplitudes, and  $\delta_1$  and  $\delta_2$  are the phase lags for  $F_1$  and  $F_2$ , respectively. It is possible to find the composite phase and amplitude behavior as a single sine wave by substituting Eq. (8) in

$$F_c(\omega) = A_c(\omega)\sin(\omega t + \delta_c(\omega)), \tag{9}$$

where  $A_c$  is the composite amplitude, and  $\delta_c$  is the composite phase lag (frequency-dependence in amplitudes and phase lags are dropped for brevity). Then,  $A_c$  and  $\delta_c$  are related to  $A_1$ ,  $A_2$ ,  $\delta_1$ , and  $\delta_2$  as follows:

$$A_c = \sqrt{[A_1 \sin(\delta_1) + A_2 \sin(\delta_2)]^2 + [A_1 \cos(\delta_1) + A_2 \cos(\delta_2)]^2} \text{ and}$$
 (10)

$$\delta_c = \sin^{-1}([A_1 \sin(\delta_1) + A_2 \sin(\delta_2)]/A_c). \tag{11}$$

Eqs. (10) and (11) yield  $A_c = 2A_1$  and  $\delta_c = \delta_1$  for identical indenter-foam pairs, as expected physically. Note that we used forces and stresses interchangeably in the analyses of single- and two-indenter-foam configurations. This is possible only for complete contacts where load-bearing contact areas are independent of loading. Therefore, the forces and stresses relate through a constant, and hence scaling laws are unaltered. In the following experiments, we control the deformation imposed on the indenter-foam dampers, measure forces, and calculate phase lags as a measure of damping capacity.

Eriten 13 VIB-20-1073

# 2.3 Experimental Details

We performed DMA on 12 different single-indenter-foam configurations (four types of foams × three indenter radii) and one two-indenter-foam configuration. DMA is a testing method to measure dynamic mechanical and dissipative properties of materials. Three foams ( $D_{pore} = 50$ , 90 and 200 µm) were made of polyethylene (PE) and the other ( $D_{pore} = 200 \,\mu\text{m}$ ) was made of PE-based olefin (INOAC Corp., Troy, MI). The foams were cut into circular sheets (22 mm in diameter and 2 mm in thickness) and immersed in extra virgin olive oil ( $\mu = 0.084 \, Pa \cdot s$  [38]) for more than 24 hours before testing. A universal tester (TA ElectroForce MODEL3200; TA Instruments, Eden Prairie, MN) was used to conduct DMA on the foams swollen in olive oil. This tester was equipped with force and displacement sensors along with data acquisition systems to monitor the dynamic normal force and displacement. Aluminum flat-ended cylindrical indenters with different radii ( $a = 4.75 \, \text{mm}$ , 3.15 mm, and 1.9 mm) were used to generate different contact radii. The contact radii served as characteristic diffusion lengths in loading.

Twelve single-indenter-foam configurations (Figure 3a and Eq. (7)) were characterized to show the tenability of a peak damping frequency. The scaling law  $(0.0001 < \left(\frac{D_{pore}}{a}\right)^2 < 0.01$  via Eq. (7)) predicts that the combination of the three mean pore diameters and three indenter radii (12 cases) promises two orders of magnitude variation in the peak damping frequency in a single-indenter-foam configuration.

An optimal two-indenter-foam configuration (Figure 3b and Eqs. (10-11)) was tested to validate whether it can provide rate-independent damping capacity. The optimal two-indenter-foam configuration was selected by applying a search criterion to the combined responses (Eqs. (10-11)) of two single-indenter-foam configurations. The detail of the search criterion is given in Section 3.2. In this combined configuration (Figure 3b), a 30 mm gap was left between the centers

of the rigid flat punches to minimize interactions, which ensures the applicability of the superposition principle (Eq. (8)). The selection of the gap complied with the literature showing minimal interaction effects in poroelastic contacts separated by five times the contact radius [39].

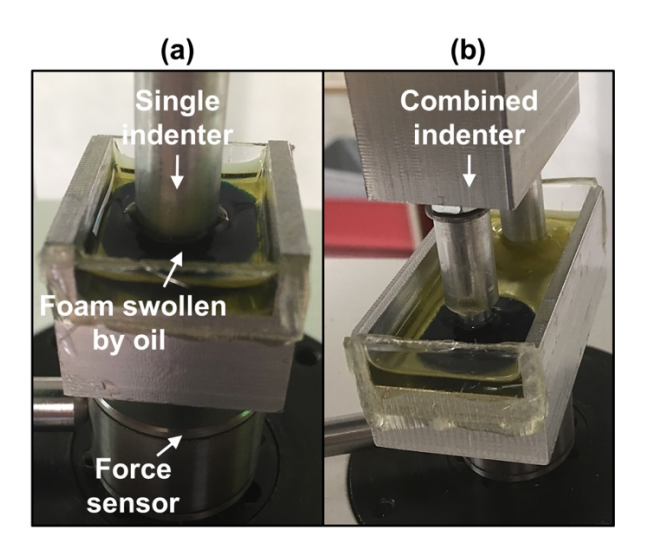


Figure 3 Images of cartilage-like PVE dampers: (a) single-indenter-foam configuration and (b) two-indenter-foam configuration. Foam sheets were immersed in olive oil during tests. The single-indenter-foam configuration was developed to demonstrate the tenability of the peak damping frequency via indenter radii a and pore diameters  $D_{pore}$ . The two-indenter-foam configuration was created to demonstrate the rate-independent damping capacity via multiple diffusion lengths in loading.

DMA was performed in a frequency range of 0.5-100 Hz by applying displacement-controlled oscillations to indenter-foam dampers, measuring reaction forces, and calculating phase lags between displacements and reaction forces. A static displacement of  $180~\mu m$  was applied to the indenter and was held for four minutes for full relaxation. Then harmonic displacements with amplitudes of around  $20~\mu m$  were applied. The static displacement was employed to ensure proper contact during tests and sufficient distance from the lower boundary of a sample. The amplitude of the harmonic indentation induced high enough excitation compared to the noise floor of the force sensor while assuring nearly linear PVE behavior (i.e., linear elastic foam response  $^+$ 

predominantly 1D radial flow of liquid phase) for all indenter-foam configurations. We varied the excitation frequency of the harmonic indentation (f = 0.5, 1, 2, 5, 10, 20, 30, 50, 75 and 100 Hz) to examine dissipative responses of foams. Two DMA measurements were performed at each frequency. Each measurement lasted for at least 59 cycles, and the last five cycles of displacement and corresponding force data were used to obtain the hysteresis loops (Figure 4c) and phase lags  $\delta$ ; i.e., a measure of damping capacity [18]. The number of cycles before the last five cycles was sufficient to reach equilibrium (Figure 4a and b). There is a minor asymmetry between the loading and unloading portions of the hysteresis loops (Figure 4c). It might stem from possible asymmetry in compression-tension response of the foams. The asymmetry remains minor for all the frequencies tested and thus is not expected to influence the damping capacity and tuning of the tested dampers. The average and standard deviation of 10 cycles (five cycles from each of the two tests) were reported. Figure 4 shows representative raw and processed DMA data. All the data was measured at the signal-to-noise ratios of more than 31 dB for the displacement data and more than 29 dB for the force data. Therefore, the level of noise is negligibly small in the recorded measurements. The raw data was processed through 4th-order lowpass Butterworth and zero-phase filters using MATLAB (The MathWorks, Inc., Natick, MA). When an excitation frequency was greater than or equal to 0.5 Hz, a filter cutoff frequency was set as 2.8 times an excitation frequency; otherwise, a cutoff frequency was set as 1 Hz. The filtfilt command of MATLAB was used to perform zero-phase filtering.

Eriten 16 VIB-20-1073

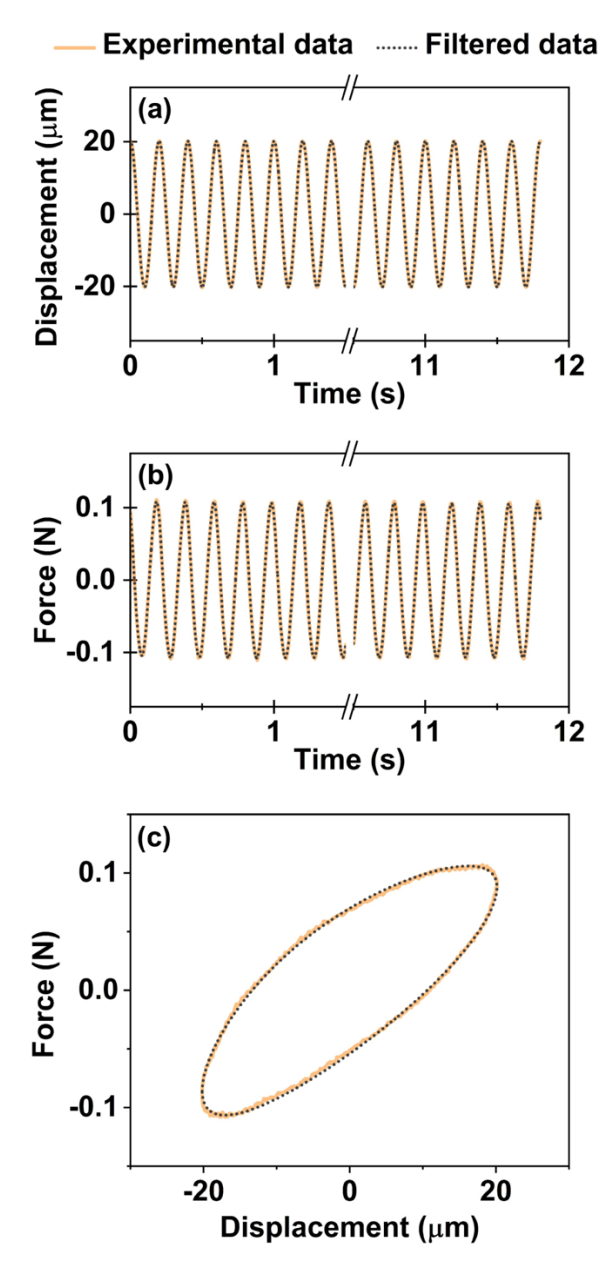


Figure 4 Representative DMA results: (a) applied displacement, (b) measured force, and (c) hysteresis loop (single cycle). The results were taken from a PE foam sheet with  $D_{pore} = 50$  µm using a single indenter with a = 4.75 mm at a frequency of 5 Hz.

# 3. RESULTS

# 3.1 Single-Indenter-Foam Configuration for Tunable Peak Damping Frequencies

The peak damping frequency of the single-indenter-foam damper was tunable across two decades by changing the combination of the pore diameter  $D_{pore}$  and indenter radius a (Figure 5).

The damping capacity of all the dampers was frequency-dependent, had a peak value, and reached a base value about two decades from the peak value. The various indenter-foam combinations generated the cartilage-inspired PVE dampers with different diffusion coefficients and characteristic diffusion lengths in loading. The alterations in a diffusion length and diffusivity enabled to shift the peak damping frequency across two decades. Regardless of the pore diameter, as the contact radius decreased, the peak damping frequency moved toward relatively high frequencies. For example, in the case of the PE foam with a pore diameter of 50 µm (Figure 5a), the peak damping frequency shifted from 1 to 5 Hz as the contact radius decreased from 4.75 mm to 1.9 mm. For a given contact radius, as the pore diameter increased, the peak damping frequency attained a higher value. For instance, when the pore diameter increased from 50 µm to 200 µm (Figure 5a-c), the peak damping frequency at a 4.75 mm contact radius shifted from 1 to 30 Hz. These observations were in line with the trend of a peak damping frequency observed in cartilage (Section 2.1). They also indicated that a peak damping frequency can be placed at a targeted frequency by controlling the diffusion and characteristic diffusion length in loading.

The tunability of the peak damping frequency in a single-indenter-foam was governed by the scaling law (Eq. (7) in Section 2.2). For a given form material (fixed pore diameter  $D_{pore}$ ), when the frequency axis was scaled with the square of the contact radius  $a^2$ , the damping capacity curves moved closer to each other (Figure 6a-d). As for the PE foam with a pore diameter of 50  $\mu$ m, the peak damping frequencies, spanning a decade from a=4.75 mm to a=1.9 mm (Figure 5a), virtually collapsed into a point after scaling (Figure 6a). Furthermore, scaling the frequency axis with the square of the ratio of a contact radius to a pore diameter  $\left(\frac{a}{D_{pore}}\right)^2$  nearly collapsed all the phase lag versus frequency curves. While the ratio of the highest to the lowest peak damping frequencies was around 100 before the scaling (Figure 5a and d), the ratio reduced to 4 after the

scaling as illustrated by the two vertical red lines in Figure 6e-h. Consequently, all the curves were centered in the vicinity of  $f\left(\frac{a}{D_{nore}}\right)^2 \cong 2 \times 10^4$  Hz and formed a master damping capacity curve. The consistency with the scaling law demonstrated that the dominant damping mechanism around the peak damping frequencies stemmed from poroelastic damping (solid-fluid interactions). Similar to cartilage damping mechanisms [27], viscoelastic damping was likely to provide damping in the tails of the damping capacity curves. Furthermore, according to the scaling law, the peak damping frequency after the scaling should be on the same order as the ratio of Young's modulus of the foams to the dynamic viscosity of the olive oil (i.e.,  $f_{peak}\left(\frac{a}{D_{nore}}\right)^2 \propto \frac{E}{\sqrt{2}\pi u}$ ). When taking the dynamic viscosity of the extra virgin olive oil as  $\mu = 0.084 \, Pa \cdot s$  [38], the scaling law leads to  $E \propto \sqrt{2}\pi\mu f_{peak} \left(\frac{a}{D_{pore}}\right)^2 \cong 10$  kPa. The storage moduli, estimated from the raw stressstrain data at 0.5 Hz, range from around 111 kPa to around 2303 kPa for all the indenter-foam configurations. Therefore, the proportionality constant to turn the scaling argument for the peak damping frequencies to an approximation for the measured values ranges from 11.1 to 230.3. Given the omission of several proportionality constants and assumptions made throughout the scaling argument, this range of proportionality constants is acceptable (see the Discussion section for details of those assumptions). A poroelastic peak damping frequency governed by the scaling law showed that a single-foam-indenter PVE damper has damping mechanisms mimicking cartilage and thus can be called a cartilage-like damper.

Eriten 19 VIB-20-1073

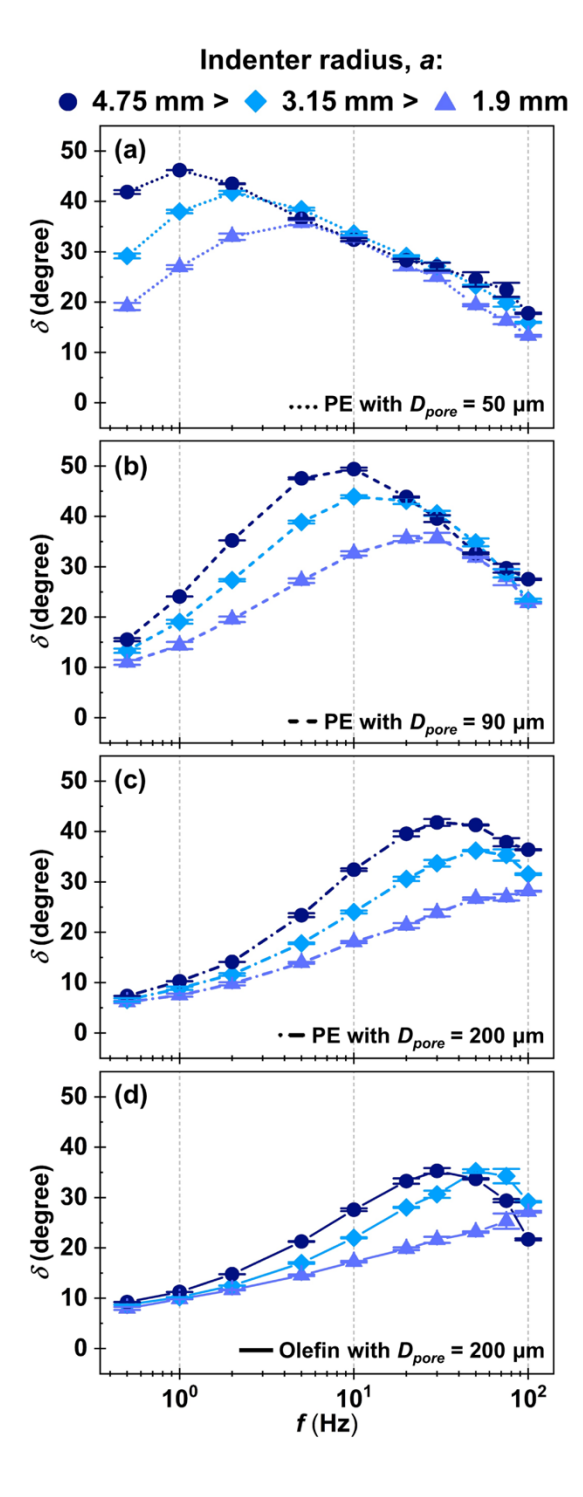


Figure 5 Phase lag  $\delta$  versus frequency f curves measured with different combinations of contact radii a, pore sizes  $D_{pore}$ , and materials. The damping capacity curves were obtained with single-indenter-foam configurations. Each subfigure shows the effect of a on  $\delta$ . The comparison of (a), (b), and (c) shows the effect of  $D_{pore}$  on  $\delta$ . The comparison between (c) and (d) presents the effect of a material on  $\delta$ .

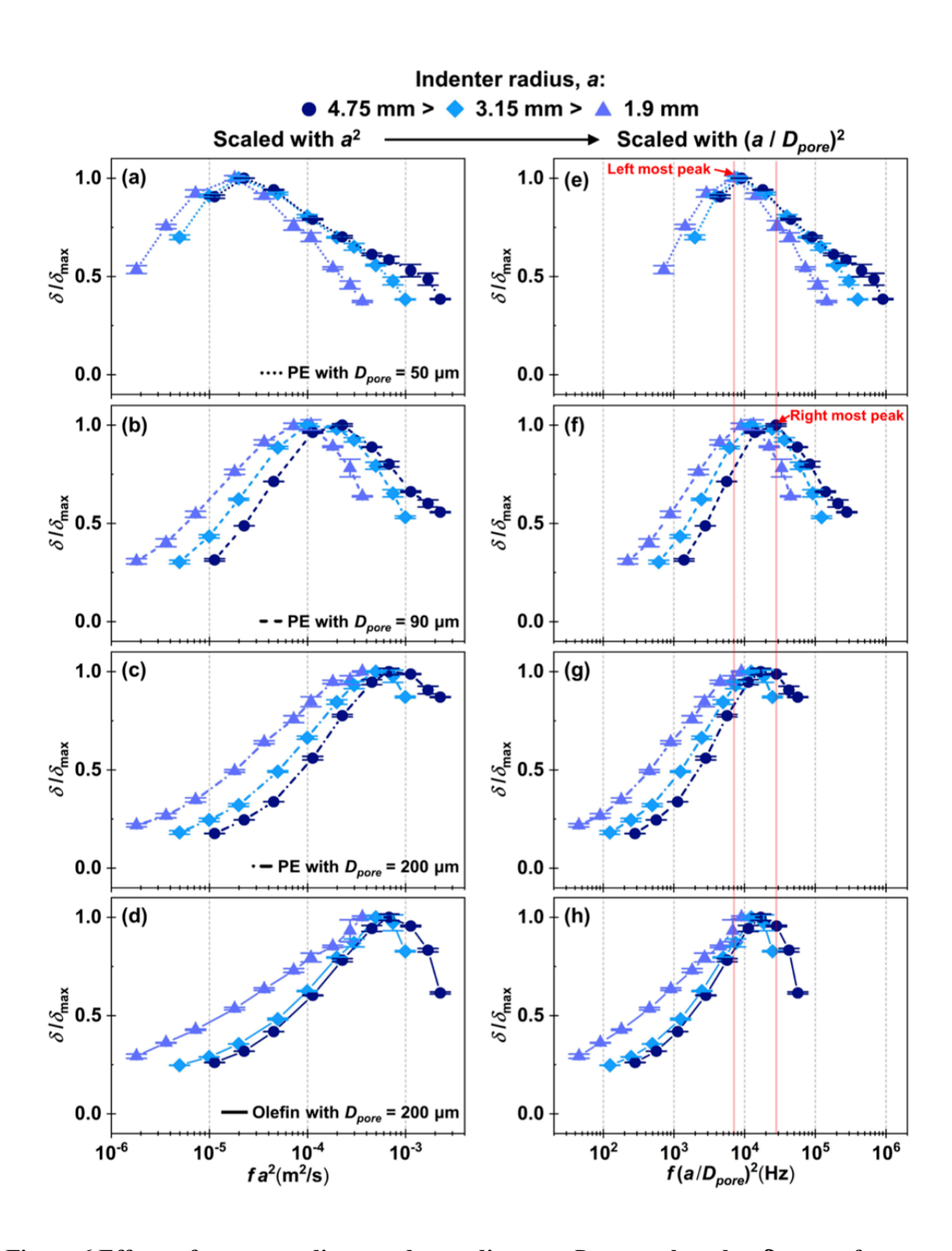


Figure 6 Effects of contact radius a and pore diameter  $D_{pore}$  on phase lag  $\delta$  versus frequency f curves. In (a-d), scaling f with  $a^2$  shifts the  $f_{peak}$  of three curves for each material (Figure 5) into a nearly single value. In (e-d), scaling  $fa^2$  with  $1/D_{pore}^2$  further aligned the  $f_{peak}$  of all

the curves with each other centering around  $f(a/D_{pore})^2 \cong 2 \times 10^4$  Hz. The red lines indicate the left and right most  $f_{peak}$  among all of the curves, and therefore stacking the curves generates a nearly single master damping curve.

# 3.2 Two-Indenter-Foam Configuration for Rate-Independent Damping Capacity

An optimal two-indenter-foam configuration for rate-independent damping capacity was obtained based on the experimental results of the single-indenter-foam configurations. After confirming that peak damping frequencies of 12 single-indenter-foam dampers were consistent with the scaling law (Eq. (7) and Section 3.1), an optimal two-indenter-foam configuration was determined by finding a combined response (Eqs. (10-11)) among 66 combinations of two-indenter-foam configurations (two out of 12 single-indenter-foam configurations), which satisfied the search criterion. The search criterion was implemented via discrete optimization and was as follows:

maximize 
$$\|\delta_c\|_{\infty}$$

subject to

$$\max \delta_c - \min \delta_c < 5^{\circ}$$

where

$$5 \text{Hz} < f < 100 \text{Hz}$$

The phase lag of an optimal two-indenter-foam configuration attains values between the phase lags of each participant indenter-foam pair because total force cannot lag more or less than force carried by either indenter. Consequently, the search criterion confirmed that the combination of  $\frac{D_{pore}}{a} = \frac{50 \, \mu m}{4.75 \, mm}$  and  $\frac{D_{pore}}{a} = \frac{200 \, \mu m}{3.15 \, mm}$  could achieve nearly rate-independent damping capacity in a frequency range of 0.5 - 100 Hz.

An optimal two-indenter-form damper provided nearly rate-independent damping capacity and was consistent with the predicted trend (Figure 7). While the damping capacity of the singleindenter-foam configurations, used for the optimal combined configuration, varied by around 26 degrees for  $D_{pore} = 50 \mu m$  with a = 4.75 mm and around 25 degrees for  $D_{pore} = 200 \mu m$  with a =3.15 mm in a frequency range of 2 - 100 Hz, the damping capacity of the two-indenter-foam configuration only varied by around 7 degrees between 2 - 100 Hz (Figure 7b); although there was a sudden drop in the damping capacity of the two-indenter-foam configuration in a frequency range of 0.5 - 2 Hz, it was still minor compared to the fluctuations in the damping capacity of the singleindenter-foam configurations. Consequently, these results showed that an optimal two-indenterfoam configuration can generate relatively rate-independent damping capacity. In addition, the trend of the rate-independent damping capacity was aligned with the predicted trend (Eqs. (10-11) and Figure 7b). Also, the experimental and predicted results were consistent with our previous simulation work in the context that selecting and combining peak damping frequencies at the bounds of the bandwidth of interest provided desired rate-independent damping capacity [33]. Hence, PVE damping in 50µm PE foam dominated the rate-independent damping capacity in the low-frequency range, whereas PVE damping in 200µm PE foam took over in the high-frequency range.

Eriten 23 VIB-20-1073

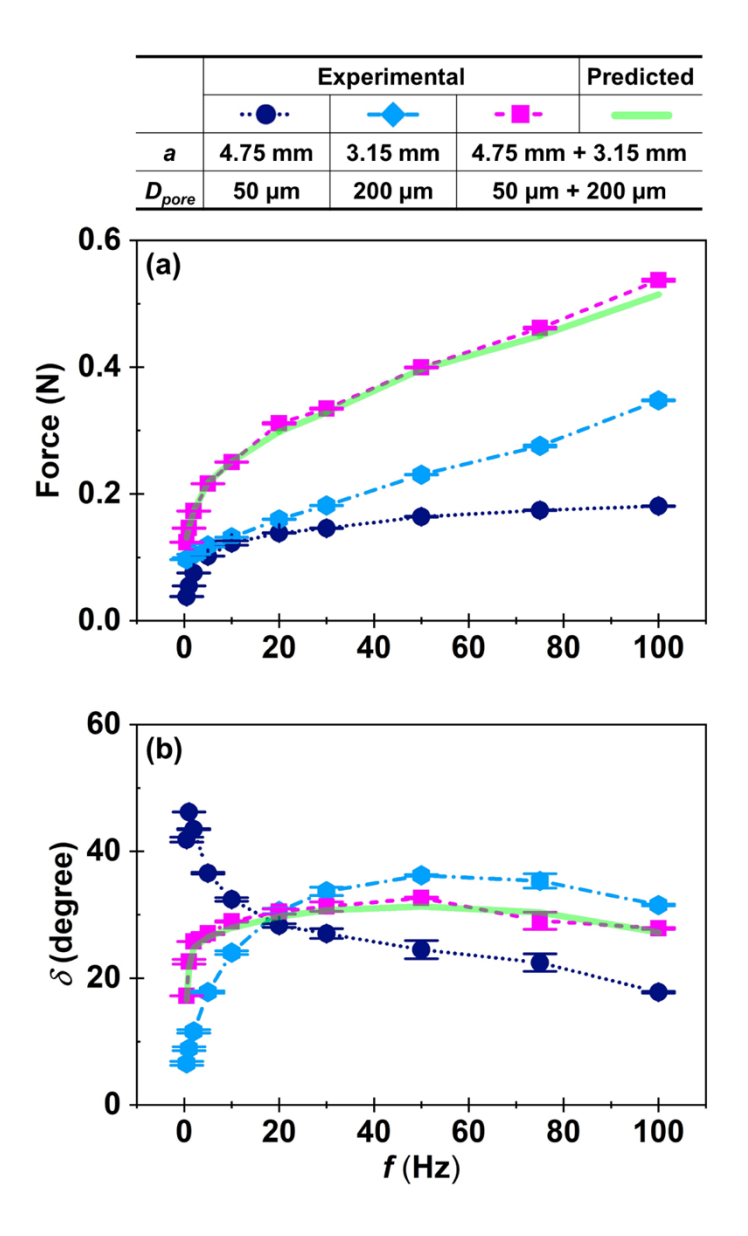


Figure 7 Force and phase lag  $\delta$  as a function of frequency f measured with single- and two-indenter-foam configurations and predicted with Eqs. (10-11): (a) force versus frequency curves and (b) phase lag versus frequency curves. The optimal two-indenter-foam configuration offered relatively rate-independent damping capacity compared to the singe-indenter-foam configuration and was consistent with the predicted curves.

# 4. DISCUSSION

This paper developed and tested passive PVE dampers inspired by cartilage damping mechanisms, allowing for the maximization of damping capacity at the desired frequency (single-indenter-foam

damper) and rate-independent damping capacity (two-indenter-foam damper). Furthermore, the scaling analysis was used to examine the peak damping capacity of the single-indenter-foam system modeled by simple constitutive relations, and it was found that the peak damping capacity was governed by the scaling law. Nevertheless, assumptions made in this scaling analysis and several practical challenges in the design of those dampers are worth revisiting.

In the scaling analysis, the foam was divided into two distinct regions. The region around the contact area was assumed to exhibit PE damping whereas the remainder was assumed to be linear elastic. This breakdown was employed to obtain a simple constitutive model for the indenterfoam damper. In reality, poroelastic diffusion gradually decreases as the stress gradient vanishes far from the contact region. Nevertheless, for cylindrical flat punches, the gradients are confined within spherical segments with radii twice as large as the contact radii [40], and therefore poroelastic effects can be safely assumed to occur in the vicinity of the contact region, within a volume that scales with the cube of contact radii. In addition, the average volumetric flux was assumed approximately equal to the liquid velocity diffusing out of that region (i.e.,  $q \approx v_l$ ). This approximation is acceptable for high porosity foams used in our experiments; the porosity of the samples ranged from 80 % to 85 %. Then, Darcy's law was used to relate flux to pressure gradient. In other words, viscous Darcian flow was assumed to dominate the liquid diffusion with negligible inertial effects (i.e., low Reynolds number  $Re = \frac{\rho_l u D_{pore}}{\mu} \ll 1$ ). In the dynamic testing presented here, the linear velocity in the vicinity of the contact region attains a maximum value of u =2 mm/s for 100 Hz cases. When the density and viscosity of olive oil and the maximum pore size are used in the experiments, the maximum Reynolds number is estimated to be around 0.002. Therefore, the Darcian flow assumption was reasonable. Lastly, the permeability and Young's modulus of the foams were assumed to be independent of applied strains. Strain-induced changes

Eriten 25 VIB-20-1073

in these properties are prominent for large strains ( $\varepsilon > 0.05$  [37]). In the dynamic testing, the deformation induced by the indenters reached 200  $\mu$ m, and this corresponded compressive strain  $\varepsilon \approx 0.07$  given the thicknesses of the foams in swollen condition. In fact, one of the factors leading to slight shifts of the damping capacity curves with respect to the scaled frequency axis (Figure 6e-h) could be the strain-induced changes in the different types of foam.

Our past numerical simulation on the multi-indenter damper configurations [33] combined with the current experimental study on the two-indenter-foam configuration showed a great degree of flexibility in tuning the broadband performance of the dampers. Notwithstanding, several design requirements have to be met before the implementation of multi-indenter-foam dampers in practice. In particular, space limitations would necessitate analyses of interacting indenters as the principle of superposition would break down for closely placed indenters. For instance, in the asymptote where most of the indenters are placed closely in clusters, poroelastic dissipation would lose efficacy, and only viscoelastic dissipation would prevail. Such configurations would lack the maximum damping performance around a peak damping frequency as viscoelastic losses are length independent, and thus should be avoided. Lastly, practical utilization of liquid-imbibed PVE materials brings inherent challenges such as leakage, contamination, temperature-pressure-shear dependent viscosity, and phase changes. Therefore, the reliable encasement of the indenter-foam dampers is essential for maintaining the desired damping capacity.

#### 5. CONCLUSION

A practical realization of cartilage-like damping capacity was demonstrated via the development of indenter-foam PVE dampers to extend damping methods in a low-frequency range (< 100 Hz). Our previous study on the numerical simulation of cartilage-like dampers [33] suggested that they have great potential to deliver effective damping capacity tailored to desired

narrow and broadband dynamic responses. This current study designed, tested, and analyzed cartilage-inspired PVE dampers in a frequency range of 0.5 – 100 Hz, employing a hybrid of interfacial and material damping. The simple mechanical model and scaling analysis provided physical parameters that govern a poroelastic peak damping frequency of a single-indenter-foam damper. The measured damping capacity of 12 single-indenter-foam dampers were consistent with the scaling analysis and demonstrated an ability to maximize poroelastic damping at the desired frequency across two decades by changing the pore diameter (diffusion) and contract radius (characteristic diffusion length). The poloelastic peak damping frequency can be tuned to specific modal frequencies of a structure so that damping is maximized only around them (narrowband performance). Viscoelastic damping was likely to provide baseline damping in a frequency range far from the poloelastic peak damping frequency. In addition, the optimized two-indenter-foam damper demonstrated that nearly rate-independent damping capacity can be achieved by combining single-indenter-foam dampers with poroelastic peak damping frequencies at the bounds of the bandwidth of interest (broadband performance). These findings on cartilage-inspired PVE dampers can appease the needs of both narrowband and broadband applications in a passive way.

## **ACKNOWLEDGEMENTS**

This work is partially supported by the National Science Foundation Grant CMMI-1662456.

## REFERENCES

- [1] U. Boz, I. Basdogan, IIR filtering based adaptive active vibration control methodology with online secondary path modeling using PZT actuators, Smart Materials and Structures. 24 (2015) 125001. https://doi.org/10.1088/0964-1726/24/12/125001.
- [2] F. Fenton, M.J. Sullivan, Cavity back iron with vibration dampening material in rear cavity, US5290036A, 1994. https://patents.google.com/patent/US5290036A/en (accessed January 31, 2020).
- [3] A.J. Keane, Passive vibration control via unusual geometries: the application of genetic algorithm optimization to structural design, Journal of Sound and Vibration. 185 (1995) 441–453. https://doi.org/10.1006/jsvi.1995.0391.
- [4] S. Behrens, A.J. Fleming, S.O.R. Moheimani, Passive vibration control via electromagnetic shunt damping, IEEE/ASME Transactions on Mechatronics. 10 (2005) 118–122. https://doi.org/10.1109/TMECH.2004.835341.
- [5] J.P. Carneal, M. Giovanardi, C.R. Fuller, D. Palumbo, Re-Active Passive devices for control of noise transmission through a panel, Journal of Sound and Vibration. 309 (2008) 495–506. https://doi.org/10.1016/j.jsv.2007.07.059.
- [6] C. Fuller, Passive distributed vibration absorbers for low frequency noise control, Noise Control Engineering Journal. 58 (2010). https://doi.org/10.3397/1.3491132.
- [7] Y. Xue, J.S. Bolton, T. Herdtle, S. Lee, R.W. Gerdes, Structural damping by lightweight poro-elastic media, Journal of Sound and Vibration. 459 (2019) 114866. https://doi.org/10.1016/j.jsv.2019.114866.
- [8] M.R.F. Kidner, C.R. Fuller, B. Gardner, Increase in transmission loss of single panels by addition of mass inclusions to a poro-elastic layer: Experimental investigation, Journal of Sound and Vibration. 294 (2006) 466–472. https://doi.org/10.1016/j.jsv.2005.11.022.
- [9] L. Zuo, S.A. Nayfeh, Optimization of the Individual Stiffness and Damping Parameters in Multiple-Tuned-Mass-Damper Systems, ASME Journal of Vibration and Acoustics. 127 (2005) 77–83. https://doi.org/10.1115/1.1855929.
- [10] L. Zuo, S.A. Nayfeh, The Two-Degree-of-Freedom Tuned-Mass Damper for Suppression of Single-Mode Vibration Under Random and Harmonic Excitation, ASME Journal of Vibration and Acoustics. 128 (2006) 56–65. https://doi.org/10.1115/1.2128639.
- [11] I.M. Koç, A. Carcaterra, Z. Xu, A. Akay, Energy sinks: Vibration absorption by an optimal set of undamped oscillators, Journal of the Acoustical Society of America. 118 (2005) 3031–3042. https://doi.org/10.1121/1.2074807.
- [12] A. Carcaterra, A. Akay, Theoretical foundations of apparent-damping phenomena and nearly irreversible energy exchange in linear conservative systems, Journal of the Acoustical Society of America. 121 (2007) 1971–1982. https://doi.org/10.1121/1.2697030.
- [13] A. Carcaterra, A. Akay, C. Bernardini, Trapping of vibration energy into a set of resonators: Theory and application to aerospace structures, Mechanical Systems and Signal Processing. 26 (2012) 1–14. https://doi.org/10.1016/j.ymssp.2011.05.005.
- [14] R.L. Weaver, The effect of an undamped finite degree of freedom "fuzzy" substructure: Numerical solutions and theoretical discussion, Journal of the Acoustical Society of America. 100 (1996) 3159–3164. https://doi.org/10.1121/1.417194.
- [15] E.E. Ungar, The status of engineering knowledge concerning the damping of built-up structures, Journal of Sound and Vibration. 26 (1973) 141–154. https://doi.org/10.1016/S0022-460X(73)80210-X.

- [16] B.J. Lazan, Damping of Materials and Members in Structural Mechanics, Pergamon Press, 1966.
- [17] K.Y. Sanliturk, D.J. Ewins, A.B. Stanbridge, Underplatform Dampers for Turbine Blades: Theoretical Modeling, Analysis, and Comparison With Experimental Data, Journal of Engineering for Gas Turbines and Power. 123 (2001) 919–929. https://doi.org/10.1115/1.1385830.
- [18] P.R. Lakes, Viscoelastic Materials, 1 edition, Cambridge University Press, Cambridge; New York, 2009.
- [19] Z. Li, M.J. Crocker, A Review on Vibration Damping in Sandwich Composite Structures, International Journal of Acoustics and Vibrations. 10 (2005). https://doi.org/10.20855/ijav.2005.10.4184.
- [20] X.Q. Zhou, D.Y. Yu, X.Y. Shao, S.Q. Zhang, S. Wang, Research and applications of viscoelastic vibration damping materials: A review, Composite Structures. 136 (2016) 460–480. https://doi.org/10.1016/j.compstruct.2015.10.014.
- [21] M. Kumar, R.A. Shenoi, S.J. Cox, Experimental validation of modal strain energies based damage identification method for a composite sandwich beam, Composites Science and Technology. 69 (2009) 1635–1643. https://doi.org/10.1016/j.compscitech.2009.03.019.
- [22] A.P. Mouritz, E. Gellert, P. Burchill, K. Challis, Review of advanced composite structures for naval ships and submarines, Composite Structures. 53 (2001) 21–42. https://doi.org/10.1016/S0263-8223(00)00175-6.
- [23] J. Park, D.L. Palumbo, Damping of Structural Vibration Using Lightweight Granular Materials, Experimental Mechanics. 49 (2009) 697–705. https://doi.org/10.1007/s11340-008-9181-x.
- [24] T. Pritz, Five-parameter fractional derivative model for polymeric damping materials, Journal of Sound and Vibration. 265 (2003) 935–952. https://doi.org/10.1016/S0022-460X(02)01530-4.
- [25] R.L. Harne, On the linear elastic, isotropic modeling of poroelastic distributed vibration absorbers at low frequencies, Journal of Sound and Vibration. 332 (2013) 3646–3654. https://doi.org/10.1016/j.jsv.2013.02.002.
- [26] S.S. Deshmukh, G.H. McKinley, Adaptive energy-absorbing materials using field-responsive fluid-impregnated cellular solids, Smart Materials and Structures. 16 (2007) 106–113. https://doi.org/10.1088/0964-1726/16/1/013.
- [27] G. Han, C. Hess, M. Eriten, C.R. Henak, Uncoupled poroelastic and intrinsic viscoelastic dissipation in cartilage, Journal of the Mechanical Behavior of Biomedical Materials. 84 (2018) 28–34. https://doi.org/10.1016/j.jmbbm.2018.04.024.
- [28] P. Kannus, Structure of the tendon connective tissue, Scandinavian Journal of Medicine & Science in Sports. 10 (2000) 312–320. https://doi.org/10.1034/j.1600-0838.2000.010006312.x.
- [29] V.C. Mow, A. Ratcliffe, A. Robin Poole, Cartilage and diarthrodial joints as paradigms for hierarchical materials and structures, Biomaterials. 13 (1992) 67–97. https://doi.org/10.1016/0142-9612(92)90001-5.
- [30] G. Han, M. Eriten, C.R. Henak, Rate-dependent crack nucleation in cartilage under microindentation, Journal of the Mechanical Behavior of Biomedical Materials. 96 (2019) 186–192. https://doi.org/10.1016/j.jmbbm.2019.04.015.

- [31] B.K. Connizzo, A.J. Grodzinsky, Tendon exhibits complex poroelastic behavior at the nanoscale as revealed by high-frequency AFM-based rheology, Journal of Biomechanics. 54 (2017) 11–18. https://doi.org/10.1016/j.jbiomech.2017.01.029.
- [32] H.T. Nia, L. Han, Y. Li, C. Ortiz, A. Grodzinsky, Poroelasticity of Cartilage at the Nanoscale, Biophysical Journal. 101 (2011) 2304–2313. https://doi.org/10.1016/j.bpj.2011.09.011.
- [33] L. Liu, A.D. Usta, M. Eriten, A broadband damper design inspired by cartilage-like relaxation mechanisms, Journal of Sound and Vibration. 406 (2017) 1–14. https://doi.org/10.1016/j.jsv.2017.06.010.
- [34] U. Boz, M. Eriten, A numerical investigation of damping in fuzzy oscillators with poroelastic coating attached to a host structure, Journal of Sound and Vibration. 417 (2018) 277–293. https://doi.org/10.1016/j.jsv.2017.12.008.
- [35] H.T. Nia, I.S. Bozchalooi, Y. Li, L. Han, H.-H. Hung, E. Frank, K. Youcef-Toumi, C. Ortiz, A. Grodzinsky, High-Bandwidth AFM-Based Rheology Reveals that Cartilage is Most Sensitive to High Loading Rates at Early Stages of Impairment, Biophysical Journal. 104 (2013) 1529–1537. https://doi.org/10.1016/j.bpj.2013.02.048.
- [36] K.L. Johnson, Contact Mechanics, Cambridge University Press, 1987.
- [37] L.J. Gibson, M.F. Ashby, Cellular Solids: Structure and Properties, Cambridge University Press, 1999.
- [38] C. Peri, The extra-virgin olive oil chain, in: Extra-Virgin Olive Oil Handbook, John Wiley & Sons, Ltd, 2014: pp. 3–10. https://doi.org/10.1002/9781118460412.ch1.
- [39] Q. Lan, A.P.S. Selvadurai, Interacting indentors on a poroelastic half-space, Zeitschrift fur Angewandte Mathematik und Physik. 47 (1996) 695–716. https://doi.org/10.1007/BF00915270.
- [40] A.C. Fischer-Cripps, Introduction to contact mechanics, 2<sup>nd</sup> ed, Springer, New York, 2007.

## **List of Figures**

Figure 2 (a) Single-indenter-foam configuration, (b) its mechanical model, and (c) two-indenter-foam configuration. Foam sheets are swollen by fluid. The damping capacity of indenter-foam dampers, inspired by cartilage mechanisms, can be tuned by controlling the contact radius a, pore diameter  $D_{pore}$ , and the number of indenters. a is a characteristic diffusion length in an indenter-foam damper. This figure is not drawn to scale.

Figure 5 Phase lag  $\delta$  versus frequency f curves measured with different combinations of contact radii a, pore sizes  $D_{pore}$ , and materials. The damping capacity curves were obtained with single-indenter-foam configurations. Each subfigure shows the effect of a on  $\delta$ . The comparison of (a), (b), and (c) shows the effect of  $D_{pore}$  on  $\delta$ . The comparison between (c) and (d) presents the effect of a material on  $\delta$ .

Figure 6 Effects of contact radius a and pore diameter  $D_{pore}$  on phase lag  $\delta$  versus frequency f curves. In (a-d), scaling f with  $a^2$  shifts the fpeak of three curves for each material (Figure 5) into a nearly single value. In (e-d), scaling  $fa^2$  with  $1/D_{pore}^2$  further aligned the  $f_{peak}$  of all the curves with each other centering around f  $(a/D_{pore})^2 \cong 2 \times 10^4$  Hz. The red lines indicate the left and right most  $f_{peak}$  among all of the curves, and therefore stacking the curves generates a nearly single master damping curve.

Figure 7 Force and phase lag  $\delta$  as a function of frequency f measured with single- and two-indenter-foam configurations and predicted with Eqs. (10-11): (a) force versus frequency curves and (b) phase lag versus frequency curves. The optimal two-indenter-foam configuration offered relatively rate-independent damping capacity compared to the singe-indenter-foam configuration and was consistent with the predicted curves.